

# Mass-15 nuclei and predicting narrow states beyond the proton drip line.

P. R. Fraser<sup>(1),\*</sup> K. Amos<sup>(2,4),†</sup> L. Canton<sup>(3),‡</sup> S. Karataglidis<sup>(4),§</sup> D. van der Knijff<sup>(2),¶</sup> and J. P. Svenne<sup>(5)\*\*</sup>

<sup>(1)</sup> *Trinity College, University of Melbourne, Victoria 3010, Australia*

<sup>(2)</sup> *School of Physics, University of Melbourne, Victoria 3010, Australia*

<sup>(3)</sup> *Istituto Nazionale di Fisica Nucleare, Sezione di Padova, via Marzolo 8, Padova I-35131, Italia,*

<sup>(4)</sup> *Department of Physics, University of Johannesburg,  
P.O. Box 524 Auckland Park, 2006, South Africa and*

<sup>(5)</sup> *Department of Physics and Astronomy, University of Manitoba,  
and Winnipeg Institute for Theoretical Physics, Winnipeg, Manitoba, Canada R3T 2N2*

(Dated: October 18, 2018)

In a previous letter (Phys. Rev. Lett. 96, 072502 (2006)), the multi-channel algebraic scattering (MCAS) technique was used to calculate spectral properties for proton-unstable  $^{15}\text{F}$  and its mirror,  $^{15}\text{C}$ . MCAS achieved a close match to the then-new data for  $p+^{14}\text{O}$  elastic scattering and predicted several unusually narrow resonances at higher energies.

Subsequently, such narrow resonance states were found. New cross section data has been published characterising the shape of the  $J^\pi = \frac{1}{2}^-$  resonance. Herein we update that first MCAS analysis and its predictions. We also study the spectra of the set of mass-15 isobars,  $^{15}\text{C}$ ,  $^{15}\text{N}$ ,  $^{15}\text{O}$ , and  $^{15}\text{F}$ , using the MCAS method and seeking a consistent Hamiltonian for clusterisation with a neutron and a proton, separately, coupled to core nuclei  $^{14}\text{C}$  and  $^{14}\text{O}$ .

PACS numbers: 21.10.Hw, 25.30.Dh, 25.40.Ep, 25.80.Ek, 24.10.-i, 25.40.Dn, 25.40.Ny, 28.20.Cz

## I. INTRODUCTION

The low-energy spectra of exotic, light-mass nuclei beyond the drip lines have been the foci of intense research efforts since the advent of radioactive ion beams. The nucleus  $^{15}\text{F}$  has been of special interest both as it spontaneously emits a proton, and for the role played by that reaction in the  $2p$ -decay of  $^{16}\text{Ne}$ .

Herein we report on results of calculations of the low energy spectra of the mass-15 isobars,  $^{15}\text{C}$ ,  $^{15}\text{N}$ ,  $^{15}\text{O}$ , and  $^{15}\text{F}$ . These nuclei are disparate in that  $^{15}\text{O}$  and  $^{15}\text{N}$  have deep binding and many fully bound states in their low energy spectra, while  $^{15}\text{C}$  is weakly bound with only two subthreshold (to neutron emission) states and  $^{15}\text{F}$  is unbound (to proton emission). To describe the low energy spectra of these systems with a single, simple, Hamiltonian is the difficult aim we set. However, a primary focus under this aim is to predict the existence and location of more states in the exotic nucleus,  $^{15}\text{F}$ , than are currently known. Regarding this nucleus, in 2002 a  $p+^{14}\text{O}$  Wood-Saxon potential was parameterised [1] to find the energies and widths of the only two  $^{15}\text{F}$  states

then known; the ground  $J^\pi = \frac{1}{2}^+$  and first excited  $\frac{5}{2}^+$  resonances. That potential, used in a three-body model for  $^{16}\text{Ne}$ , proved useful in recent analyses of 2-proton decay data [2, 3]. In 2004, the first  $^{14}\text{O}(p,p)^{14}\text{O}$  cross section data taken at several angles and at energies spanning the two known resonance states was published [4]. In that paper, data fits found using Woods-Saxon potentials were shown. The next year, this data was analysed with a microscopic cluster model, which obtained a good match [5], and further data was soon taken and published [6]. In the same year, properties of these two  $^{15}\text{F}$  states were studied with a simplistic shell model [7]. This model was restricted to the lowest three configurations of one-particle/two-hole and three-particle/four-hole, states.

In 2006, the multichannel algebraic scattering method (MCAS) was used to analyse the data of Refs. [4, 6], defining potentials between  $^{14}\text{O}$  and protons from a collective model with rotor character, while accounting for the Pauli principle between the proton and the underlying  $^{14}\text{O}$  shell structure [8]. As well as obtaining a close fit with the cross-section data, the MCAS calculation predicted narrow resonances at higher energies. These were a  $\frac{1}{2}^-$  state with energy (width) of 5.49 (0.005) MeV, a  $\frac{5}{2}^-$  of 6.88 (0.01) MeV, a  $\frac{3}{2}^-$  of 7.25 (0.04) MeV, as well as  $\frac{1}{2}^+$ ,  $\frac{5}{2}^+$  and  $\frac{3}{2}^+$  states of 7.21 (1.2), 7.75 (0.4) and 7.99 (3.6) MeV, respectively.

The width of such narrow states caused some controversy [9, 10] (with Ref. [9] using a potential model to construct broad single-particle resonances whose widths were manually scaled down by over an order of magnitude

\*Electronic address: paulfr@trinity.unimelb.edu.au

†Electronic address: amos@unimelb.edu.au

‡Electronic address: luciano.canton@pd.infn.it

§Electronic address: stevenka@uj.ac.za

¶Electronic address: dvanderknijff@gmail.com

\*\*Electronic address: svenne@physics.umanitoba.ca

to fit data for narrow resonances). Subsequently however, the existence of the states predicted by the MCAS calculation has been verified experimentally [11–13]. (Note that in Table I of Ref. [13], the labels for results reproduced from Ref. [8] and [9] were accidentally switched.) For completeness we note that the afore-mentioned simple shell model calculation was revised [14] in the light of the new data.

Narrow states have now been observed in other proton rich nuclei, e.g.  $^{19}\text{Na}$  [15],  $^{16}\text{Ne}$  [13],  $^{15}\text{Ne}$  [16], and  $^{23}\text{Al}$  [17], with narrow resonances of the latter found with an MCAS study [18]. They have been predicted for  $^{21}\text{Al}$  [19] and  $^{25}\text{P}$  [20]. Such narrow resonances indicate an eigenstate with structure which has little overlap with the ground state. In the case at hand, this is the difference between a one-proton emitting clusterization ( $p+^{14}\text{O}$ ) and a two-proton emitting clusterization ( $2p+^{13}\text{N}$ ). Pauli hindrance accounts for this effect [21].

Recent developments include the publication of more complete data with smaller uncertainties over a larger energy range [22–24]. Where Ref. [13] provided evidence of the narrow  $\frac{1}{2}^-$  resonance predicted by MCAS, Ref. [24] provides details of its shape, finding it to be a dip in cross section, as did our first MCAS calculation. Further, in Ref. [24] and in a recently-published thesis [25], the coupled-channels Gamow shell model (GSM-CC) [26] has been used to calculate the  $^{14}\text{O}(p,p)^{14}\text{O}$  cross section in the energy range of that data, reproducing the  $\frac{1}{2}^+$ ,  $\frac{5}{2}^+$  and  $\frac{1}{2}^-$  resonances well. At higher energies, that calculation slightly underestimates experiment.

As MCAS theory has undergone a decade of refinement since Ref. [8], we now take the opportunity presented by this new data to revisit our calculation in the energy range where cross sections have been measured and beyond, where MCAS predicts further resonances. Section II summarises the MCAS method and details improvements since the work of Ref. [8]. Section III presents calculated results for the spectra of the mirror systems  $^{15}\text{C}$  and  $^{15}\text{F}$ . Section IV shows the new  $p+^{14}\text{O}$  cross section results compared to recent data. In Section V, we investigate how many details of the spectra of another mass-15 mirror pair,  $^{15}\text{O}$  and  $^{15}\text{N}$ , may be described by essentially the same nuclear potential, i.e. that for  $n+^{14}\text{O}$  and  $p+^{14}\text{C}$ . Finally, conclusions are drawn in Section VI.

## II. DETAILS OF THE METHOD

The method finds solutions of coupled-channel Lippmann-Schwinger equations in momentum space using finite-rank expansions of an input matrix of nucleon-nucleus interactions. A set of Sturmian functions is used as expansion basis and this allows locating all compound-system resonance centroids and widths, regardless of how narrow, and by using negative energies, allows determination of sub-threshold bound states. Further, use of or-

thogonalizing pseudopotentials (OPP) in generating the Sturmians ensures that the Pauli principle is not violated [27, 28], even with a collective-model formulation of nucleon-nucleus interactions. Otherwise, some compound nucleus wave functions may possess spurious components [29].

Results we have obtained vary slightly from those previously published [8] since five target (or core) nuclear states now have been used in the coupled-channel evaluations (rather than the three in Ref. [8]), and so the interaction potential parameters have been adjusted slightly, and exact masses of the nucleons and nuclei used rather than the mass numbers. Further, the Coulomb interactions in the  $p+^{14}\text{O}$  cluster has been derived from a three parameter Fermi (3pF) form for the charge distribution in  $^{14}\text{O}$ , adding to the nuclear interaction which has the form

$$V_{cc'}(r) = \left[ \{V_0 + V_U \ell \cdot \ell\} f(r, R, a) + V_{\ell \cdot s} \frac{df(r, R, a)}{dr} \ell \cdot s \right]_{cc'}. \quad (1)$$

Here  $f(r, R, a)$  is a deformed Woods-Saxon function, and both quadrupole and octupole deformations are taken to second order in specifying the coupled-channel ( $c, c'$ ) potentials.

For full details, see [27, 30, 31].

### A. States used for the core nuclei, $^{14}\text{C}$ and $^{14}\text{O}$

In Fig. 1, the known low-energy spectra of the mirror nuclei  $^{14}\text{C}$  and  $^{14}\text{O}$  are shown. These states have all been used in the current coupled-channel calculations. While the sequence of each of the states shown (the spin-parities) are as required by the mirror condition and the excitation energies are comparable, there are features that vary from a strict mirror arrangement. Notably, the actual excitation energies of the states in  $^{14}\text{O}$  differ from those of their matching partners in  $^{14}\text{C}$ , as do the energy gaps, but also the relative nucleon breakup energies are quite different; 8.176 MeV for neutron emission from  $^{14}\text{C}$  but only 4.628 MeV for a proton emission from  $^{14}\text{O}$ . Consequently the four excited states in  $^{14}\text{O}$  are resonances while those in  $^{14}\text{C}$  are not. The widths of the four  $^{14}\text{O}$  resonances are shown in brackets in Fig. 1 and the units are MeV. The asterisk with the width of the first excited ( $1^-$ ) resonance indicates that its emission form is not identified in the tabulation used [32]. The other three all decay by proton emission. For details of how MCAS treats core nuclei states which are themselves resonances, see Refs. [31, 33, 34]. This represents another upgrade with respect to the calculation originally published [8].

As the two cores used in these coupled-channel, nucleon-nucleus cluster calculations do not show perfect mirror symmetry even at low excitation, one may expect the possibility of some asymmetry between the two

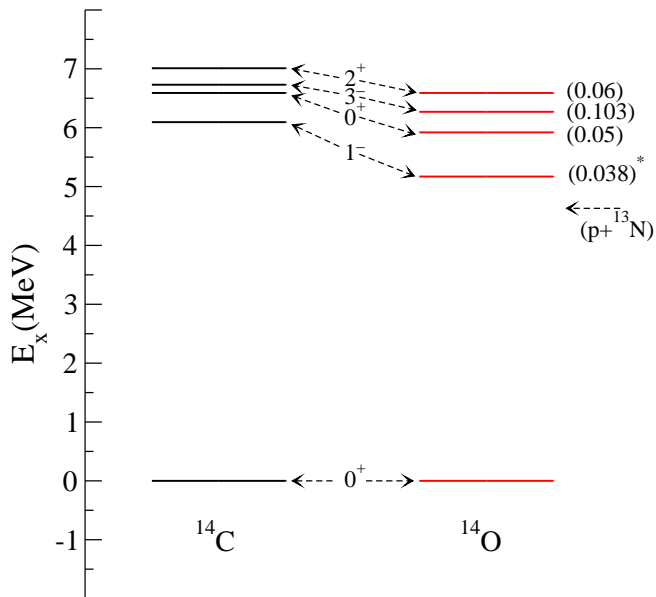


FIG. 1: The low excitation spectra of the mass-14 mirror nuclei,  $^{14}\text{C}$  and  $^{14}\text{O}$ , used in MCAS calculations. The spin-parities of the states are listed in the middle of the diagram.

Hamiltonians required to best define the relative mass-15 spectra, in addition to simply a Coulomb interaction added to the cluster model Hamiltonian that best describes the  $^{15}\text{C}$  spectrum. Some added asymmetry may be due to a charge dependence of the strong force. With the  $NN$  interaction, evidence for charge-symmetry and charge-independence breaking is given by the results of scattering experiments; asymmetry has been noted with scattering lengths, namely

$$a_{pp}^N - a_{nn}^N = 1.65 \pm 0.60, \quad (2)$$

and

$$(a_{pp}^N + a_{nn}^N)/2 - a_{np}^N = 5.6 \pm 0.6. \quad (3)$$

The first indicates a small difference between  $v_{pp}^N$  and  $v_{nn}^N$  implying a charge-symmetry breaking, while the second, is evidence of the breaking of charge-independence. So  $NN$  forces have a charge dependence and that suggests there may be a non-negligible isospin-symmetry breaking component of the effective  $NN$  interaction to be used in models of nuclear structure. The isospin non-conserving (INC) shell model [35] is an example.

When considering how much charge dependence may affect differences between the two mirror nuclei considered, it is important to take into account that  $^{14}\text{C}$  has an unusually large log-ft value of 9.04. Its mirror,  $^{14}\text{O}$ , has a value of 3.4892. Thus, while the difference in ground state energies is only 80 keV, the wave functions may not be exact mirrors. The spectra are similar, but the first excited state energies differ by 920 keV. As a result, while this indicates that there may be a difference in energy due to Coulomb effects one cannot estimate it with any certainty due to the anomalous log-ft value for  $^{14}\text{C}$ .

No shell model wave function has been able to reproduce that large value [36].

In this investigation, these differences are taken into account by (small) variations in the OPP. (See Section II C.)

## B. The charge distribution and electromagnetic properties

For any nuclear charge distribution, electric multipole operators are defined in the space-fixed frame by

$$T_{\lambda\mu} = \int \rho_{ch}(\mathbf{r}) r^\lambda Y_{\lambda\mu}^*(\theta, \phi) d\mathbf{r}. \quad (4)$$

Here  $\mu\hbar$  is the angular momentum projection on the space-fixed z-axis.

We suppose that the nucleus is like an incompressible liquid drop whose surface,  $R(\theta, \phi)$ , can be deformed. Expanding that surface to first order gives

$$R(\theta\phi) = R_0 \left[ 1 + \sum_{\lambda\mu} \alpha_{\lambda\mu}^* Y_{\lambda\mu}(\theta\phi) \right]. \quad (5)$$

Then any function with that surface can also be expanded as

$$F(\mathbf{r}) = F(r) - R_0 \frac{dF}{dr} \sum_{\lambda\mu} \alpha_{\lambda\mu}^* Y_{\lambda\mu}(\theta\phi), \quad (6)$$

and, in particular, the nuclear charge distribution as

$$\rho_{ch}(\mathbf{r}) = \rho_0 \rho_{ch}(r) - \rho_0 R_0 \left( \frac{d\rho_{ch}(r)}{dr} \right) \sum_{lm} \alpha_{lm}^* Y_{lm}(\Omega). \quad (7)$$

Here  $\rho_0$  is the central charge density value,  $\rho_0 = Ze / [4\pi \int \rho_{ch}(r) r^2 dr]$ .

Substituting Eq. (7) in Eq. (4) gives

$$\begin{aligned} T_{\lambda\mu} &= \int \rho_{ch}(\mathbf{r}) r^\lambda Y_{\lambda\mu}^*(\theta\phi) d\mathbf{r} \\ &= -\rho_0 R_0 \int_0^\infty r^{\lambda+2} \left( \frac{d\rho_{ch}(r)}{dr} \right) dr \alpha_{\lambda\mu}^*. \end{aligned} \quad (8)$$

Quantisation with the collective vibration model is then made using the transformation

$$\alpha_{\lambda\mu}^* \rightarrow \beta_\lambda \frac{1}{\sqrt{(2\lambda+1)}} \left\{ b_{\lambda\mu}^\dagger + (-)^\mu b_{\lambda-\mu} \right\}; \quad (9)$$

$b_{\lambda\mu}^\dagger$  and  $b_{\lambda-\mu}$  are phonon creation and annihilation operators and  $\beta_\lambda$  are coupling strengths.

First order expansions suffice for transitions between pure vibration model states; the ground as the vacuum ( $|0, 0\rangle$ ), and the  $2_1^+$  and  $3_1^-$  ones being a single quadrupole and single octupole phonon excitation upon that vacuum,  $b_{2\mu}^\dagger |0, 0\rangle$  and  $b_{3\nu}^\dagger |0, 0\rangle$  respectively. Electromagnetic transitions between the ground state and the

single phonon excited states have matrix elements of the form

$$\begin{aligned} & \langle J_f M_f | \alpha_{J_f M_f}^* | 0, 0 \rangle \\ &= \left\langle 0, 0 \left| b_{J_f M_f} \beta_\lambda \frac{1}{\sqrt{2J_f + 1}} b_{J_f M_f}^\dagger \right| 0, 0 \right\rangle \\ &= \frac{1}{\sqrt{2J_f + 1}} \beta_{J_f}. \end{aligned} \quad (10)$$

with which the electromagnetic transition probabilities are

$$B(E\lambda) = \sum_{M_f} |\langle J_f M_f | T_{\lambda\mu} | 00 \rangle|^2 = |\langle J_f || T_\lambda || 0 \rangle|^2. \quad (11)$$

have  $\lambda = J_f$ . For the finite distribution of charge, these transition probabilities are given by

$$B(E\lambda) \uparrow = \frac{1}{(2J_f + 1)} \beta_{J_f}^2 \rho_0^2 R_0^2 \left[ \int_0^\infty r^{\lambda+2} \left( \frac{d\rho_{ch}(r)}{dr} \right) \right]^2. \quad (12)$$

We use this pure vibration model to describe the states of  $^{14}\text{O}$  in MCAS evaluations of the spectra of  $^{15}\text{F}$  treated as the  $p+^{14}\text{O}$  cluster, and of low-energy scattering of  $^{14}\text{O}$  ions from hydrogen. Quadrupole and octupole coupling constants are involved in defining the matrix of interaction potentials to be used and for these we usually seek guidance from electromagnetic properties of the ‘target’. The relevant  $B(E2) \uparrow$  and  $B(E3) \uparrow$  values in  $^{14}\text{O}$  are as yet unknown, while those values for the transitions in  $^{14}\text{C}$  are uncertain, though from that  $B(E2)$  value, Raman [37] gives an adopted value of  $\beta_2 = 0.36$  (the sign being ambiguous since  $B(E2)$  depends on  $\beta_2^2$ ). However, we assume that both the  $E2$  and  $E3$  transitions in  $^{14}\text{O}$  would be similar to those in  $^{16}\text{O}$ , namely  $\sim 40 \text{ e}^2\text{-fm}^4$  [37] and  $\sim (1300 - 1500) \text{ e}^2\text{-fm}^6$  [38] respectively.

We have used a 3pF model for the charge distribution in  $^{14}\text{O}$ , *viz.*

$$\rho_{ch}(r) = \frac{1 + w_c \left( \frac{r^2}{R_c^2} \right)}{1 + \exp\left( \frac{r - R_c}{a_c} \right)}. \quad (13)$$

As reported in Ref. [39], electron scattering form factors, when used to specify a 3pF charge distribution for  $^{16}\text{O}$ , set the parameter values as  $R_c, a_c, w_c = 2.608 \text{ fm}, 0.52 \text{ fm}, -0.051$ . We presuppose that the charge distribution in  $^{14}\text{O}$  would be slightly more diffuse and have used the set,  $R_c, a_c, w_c = 2.59 \text{ fm}, 0.6 \text{ fm}, -0.051$ . With that distribution, the  $B(E2) \uparrow$  with  $\beta_2 = 0.36$  is  $45.6 \text{ e}^2\text{-fm}^4$ ; cf.  $40.6 \text{ e}^2\text{-fm}^4$  adopted for the transition in  $^{16}\text{O}$ . The  $B(E3) \uparrow$  found using  $\beta_3 = 0.48$  is  $1323 \text{ e}^2 \text{ fm}^6$  which compares with the adopted value of  $1300 \text{ e}^2 \text{ fm}^6$  for  $^{16}\text{O}$  assessed from electron scattering data. For a full description of how the 3pF charge distribution is implemented in MCAS, see Refs. [18, 40].

TABLE I: Parameter values defining the  $n+^{14}\text{C}$  and  $p+^{14}\text{O}$  interaction.  $\lambda$  are blocking strengths of occupied single nucleon orbits, in MeV. Additionally, all states involve a  $\lambda$  strength of  $10^6$  for the  $1s_{\frac{1}{2}}$  orbit. The numbers in brackets are the OPP values required to give the best representation of the three low excitation states in  $^{14}\text{F}$ . Lengths are in fm.

		Odd parity	Even parity			
$V_0$ (MeV)		-48.16	-43.16			
$V_{ll}$ (MeV)		0.475	0.475			
$V_{ls}$ (MeV)		7.0	7.0			
$V_{ss}$ (MeV)		0.0	0.0			
<hr/>						
$R_0$ (fm)	$a$ (fm)	$R_c$ (fm)	$a_c$ (fm)	$w_c$	$\beta_2$	$\beta_3$
3.083	0.63	2.59	0.6	-0.051	-0.36	-0.48
<hr/>						
$J^\pi$	$E^{14}\text{C}$	$E^{14}\text{O}$	$\lambda_{p_{\frac{3}{2}}}$	$\lambda_{p_{\frac{1}{2}}}$		
$0_1^+$	0.00	0.00	$10^6$	9.9 (9.42)		
$1_1^-$	6.09	5.17	16.0	5.25		
$0_2^+$	6.59	5.92	$10^6$	4.2		
$3_1^-$	6.73	6.27	16.0	4.3 (11.75)		
$2_1^+$	7.01	6.59	$10^6$	2.5 (2.9)		

### C. Parameter values for the nuclear interaction

A vibration collective model has been used to specify the matrices of interaction potentials with the clusters,  $^{15}\text{C}$  ( $n+^{14}\text{C}$ ) and  $^{15}\text{F}$  ( $p+^{14}\text{O}$ ) as has been used recently [41]. The coupled-channel interaction matrices were formed using the five states in  $^{14}\text{C}$  and  $^{14}\text{O}$  as discussed above. They are listed again in Table I in which the strengths of the OPP terms required for each are given. The OPP scheme is one that allows for Pauli blocking or hindrance of the added nucleon to the core nucleus in forming the relevant compound nuclear system. The OPP strengths listed in Table I are those that lead to good results for the low excitation spectra for  $^{15}\text{C}$  and  $^{15}\text{F}$ . Those values, shown in brackets in the table, effect fine tuning of the energies of the  $^{15}\text{F}$  levels, notably of the  $\frac{1}{2}^-$  state. This may be a reflection of the differences between the spectra of the core nuclei,  $^{14}\text{C}$  and  $^{14}\text{O}$ .

The interaction potential strengths required in the MCAS calculations for the the nucleon - mass-14 clusters were  $V_0 = 43.16$ ,  $V_{ll} = 0.475$ , and  $V_{ls} = 7.0$  MeV. The parameter values of the nuclear interaction geometry used are,  $R_0 = 3.063 \text{ fm}$ ,  $a_0 = 0.62 \text{ fm}$ ., and the deformation parameter values used are  $\beta_2 = -0.36$  and  $\beta_3 = -0.48$ . The calculations of the  $^{15}\text{F}$  ( $p+^{14}\text{O}$ ) system required addition of Coulomb interactions, and those were derived assuming that  $^{14}\text{O}$  had the 3pF charge distribution given in Eq. (13).

### III. ENERGY LEVELS OF $^{15}\text{C}$ AND $^{15}\text{F}$

The spectra of  $^{15}\text{C}$  and of  $^{15}\text{F}$  found using MCAS are compared with the experimental values graphically in Figs. 2 and 3 respectively. They are discussed in the following subsection. The two lowest states in  $^{15}\text{C}$  are subthreshold to neutron break-up but all other states are resonances. Then in subsection III B, the centroid energies and widths, are listed in Tables II and III respectively.

#### A. Energy level diagrams

In Fig. 2, the known low-energy spectrum of  $^{15}\text{C}$  (to  $\sim 8$  MeV excitation) is shown in the column identified by ‘Expt.’. The lowest eight states have known spin-parities. They are compared with the spectral results

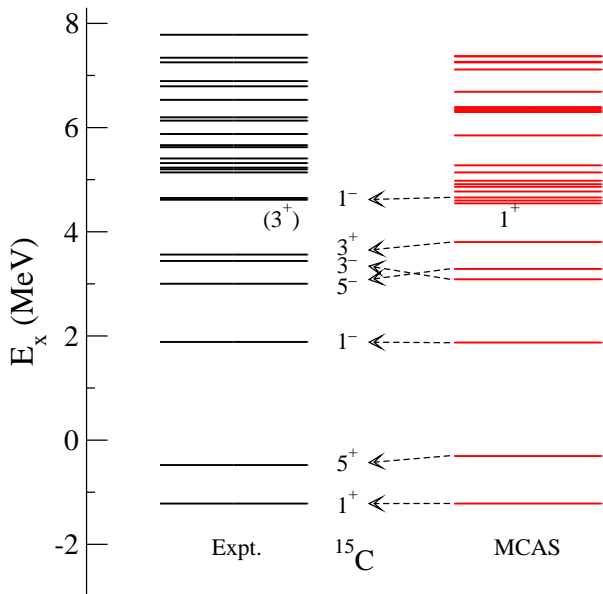


FIG. 2: Spectra of  $^{15}\text{C}$  in relation to the  $n+^{14}\text{C}$  threshold. The states are classified by twice their spin and their parity.

obtained using MCAS with the vibration model describing the interactions of a neutron with the five states of the core nucleus,  $^{14}\text{C}$ , shown in Fig. 1. All states other than the lowest two are resonances and can decay by neutron emission. The lowest six known states (to  $\sim 5$  MeV excitation in  $^{15}\text{C}$ ) are well matched by the MCAS results save that the order of the close lying  $\frac{5}{2}^-$  and  $\frac{3}{2}^-$  resonances is interchanged. The energy of the ground state lies 1.217 MeV below the  $n+^{14}\text{C}$  threshold in good agreement with the experimental value of 1.218 MeV.

As evident in Fig. 3, little is known of the spectrum of  $^{15}\text{F}$ , but the first three resonances have established spin-parity assignments consistent with the lowest three states in the mirror,  $^{15}\text{C}$ . Five states of  $^{14}\text{O}$ , the mirrors of those in  $^{14}\text{C}$ , were used in the MCAS evaluations for

$^{15}\text{F}$ . The known values of the excitation energies (four being resonance centroid energies) and the widths (of those four resonances), were taken into account in the coupled-channel calculations. The relevant Hamiltonian initially, was taken as that deemed best in giving the spectrum of  $^{15}\text{C}$  from the  $n+^{14}\text{C}$  cluster evaluation, with the addition of Coulomb interactions formed using the 3pF model of the charge distribution in  $^{14}\text{O}$ . The results of that initial evaluation are those shown in Fig. 3 and labelled therein by ‘mirror’. There is reasonable comparison with the known spectrum (‘Expt.’). Small adjustments made by variation of the  $\lambda_{p\frac{1}{2}}$  values in the OPP set give the results identified as ‘best’. Importantly both evaluations lead to the ground state resonance lying at 1.279 MeV in the  $p+^{14}\text{O}$  center of mass. Clearly there are many more states predicted to lie in the spectrum above the three, well established, resonances.

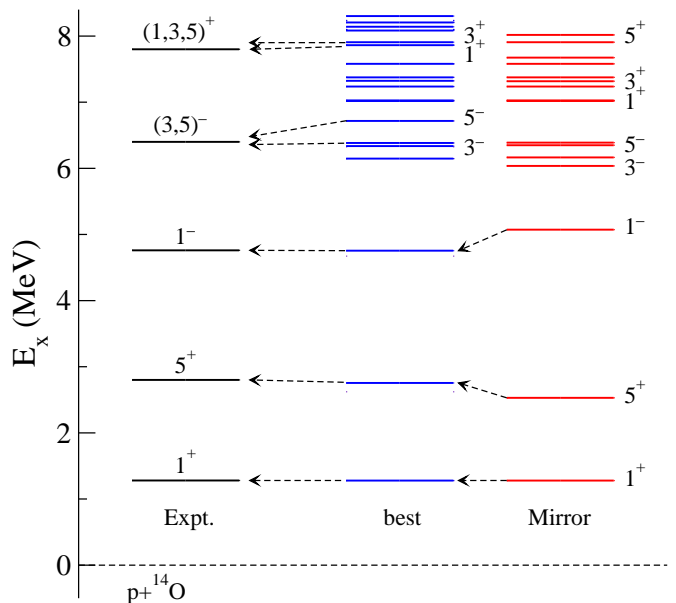


FIG. 3: Spectra of  $^{15}\text{F}$  in relation to the  $p+^{14}\text{O}$  threshold. The states are classified by twice their spin and their parity.

#### B. Tabulated level energies and widths

The two lowest states in  $^{15}\text{C}$  are subthreshold to neutron break-up but all other states are resonances. The widths determined by the MCAS evaluations are solely those for nucleon break-up of the mass-15 systems. With  $^{15}\text{F}$ , the lowest two resonances only decay by proton emission and the measured and calculated widths can be compared. We list the values for  $^{15}\text{C}$  that are given in Ref. [32] but for the three lowest states in  $^{15}\text{F}$  we have used the values assessed in a recent article [24]. (See Ref. [42] for discussion of other measured results.)

The coupled-channel (nuclear) interaction Hamiltonian and the OPP accounting for Pauli blocking and/or

TABLE II: Spectra of  $^{15}\text{C}$ . The experimental values, Expt., are compared with the MCAS results found using the vibration model. All resonance centroid  $E_r$  and (full) width  $\Gamma$  values are in MeV.

Expt.			MCAS		
$J^\pi$	$E_r$	$\Gamma$	$J^\pi$	$E_r$	$\Gamma$
$\frac{1}{2}^+$	<b>-1.218</b>	—	$\frac{1}{2}^+$	<b>-1.217</b>	—
$\frac{5}{2}^+$	<b>-0.478</b>	—	$\frac{5}{2}^+$	<b>-0.3056</b>	—
$\frac{1}{2}^-$	<b>1.885</b>	< 0.040	$\frac{1}{2}^-$	<b>1.874</b>	0.019
$\frac{5}{2}^-$	<b>3.002</b>	< 0.014	$\frac{5}{2}^-$	<b>3.287</b>	0.003
$\frac{3}{2}^-$	<b>3.439</b>		$\frac{3}{2}^-$	<b>3.088</b>	0.028
$\frac{3}{2}^+$	<b>3.562</b>	1.74	$\frac{3}{2}^+$	<b>3.802</b>	3.16
			$\frac{1}{2}^+$	4.545	0.218
			$\frac{3}{2}^-$	4.600	0.009
$(\frac{3}{2}^+)$	<b>4.615</b>	0.064	$\frac{3}{2}^+$	<b>4.980</b>	0.337
$\frac{1}{2}^-$	<b>4.648</b>		$\frac{1}{2}^-$	<b>4.648</b>	0.006
$(\frac{5}{2}, \frac{7}{2}, \frac{9}{2}^+)$	<b>5.14</b>	< 0.02	$\frac{5}{2}^+$	<b>5.140</b>	0.297
			$\frac{5}{2}^-$	5.275	0.009
$(\frac{3}{2} \rightarrow \frac{7}{2})$	5.2	$\sim 0.05$	$\frac{1}{2}^+$	5.849	$7^{-5}$
			$\frac{7}{2}^-$	6.300	0.037
			$\frac{5}{2}^+$	6.232	0.032

hindrance in the selected five states of  $^{14}\text{C}$ , were chosen to give an optimal match to the known lowest eight states in  $^{15}\text{C}$ . To emphasise that, those with energies within  $\sim 300$  keV of the data are shown in bold face type in Table II. There are many more states predicted by this collective model evaluation. Above 5 MeV in the spectrum listed in Table II, the experimentally known resonances have ambiguous spin-parity assignments though the richer evaluated spectra have characteristics consistent with those sets. The widths of the first two resonances are small and consistent with observation.

The coupled-channel interaction potentials so found were then used with MCAS to define a spectrum for  $^{15}\text{F}$ . But, as described earlier, some essential changes to the input specifications had to be made. First most states of the mirror core nucleus,  $^{14}\text{O}$ , are in fact resonances themselves and were used as such in the MCAS evaluations. The excitation energy centroids of those states differ slightly from the corresponding ones in  $^{14}\text{C}$ . Then there are Coulomb interactions to be included with the  $p$ - $^{14}\text{O}$  cluster evaluations. To find the best representation of the  $^{15}\text{F}$  spectrum, small adjustments to the  $\lambda_{p\frac{1}{2}}$  OPP values as indicated in Table I, were made. The results are given in Table III where they are compared with the limited known spectral values [13, 24].

The three best determined resonances, centroid energies and widths, are quite well matched by the calculation results as are the other two higher excitation resonances that have uncertain spin-parities and widths. The widths of the resonances found with MCAS link solely to

TABLE III: Spectra of  $^{15}\text{F}$ . The notation is as given in Table II. N.B.: In Ref. [13], Table I gives widths for their  $(\frac{5}{2}, \frac{3}{2})^-$  state as 0.2(2), the text on page 10 indicates that 0.2 MeV is the experimental resolution.

Expt.				MCAS		
Ref.	$J^\pi$	$E_r$	$\Gamma$	$J^\pi$	$E_r$	$\Gamma$
[24]	$\frac{1}{2}^+$	<b>1.270</b>	$0.376 \pm 0.070$	$\frac{1}{2}^+$	<b>1.280</b>	0.708
[24]	$\frac{5}{2}^+$	<b>2.794</b>	$0.30 \pm 0.010$	$\frac{5}{2}^+$	<b>2.651</b>	0.336
[24]	$\frac{1}{2}^-$	<b>4.757</b>	$0.036 \pm 0.014$	$\frac{1}{2}^-$	<b>4.755</b>	0.106
				$\frac{3}{2}^-$	6.148	0.286
				$\frac{1}{2}^-$	6.336	0.509
				$\frac{3}{2}^-$	<b>6.384</b>	0.951
[13]	$(\frac{3}{2}, \frac{5}{2}^-)$	<b>6.4</b>	$\leq 0.2$	$\frac{5}{2}^-$	<b>6.717</b>	0.074
				$\frac{1}{2}^+$	7.018	0.257
				$\frac{7}{2}^-$	7.027	0.176
				$\frac{5}{2}^-$	7.323	0.145
				$\frac{3}{2}^+$	7.376	0.155
				$\frac{1}{2}^-$	7.580	0.062
				$\frac{1}{2}^+$	7.862	0.052
[13]	$(\frac{3}{2}, \frac{5}{2}^+)$	<b>7.8</b>	$0.4 \pm 0.4$	$\frac{3}{2}^+$	<b>7.906</b>	0.134
				$\frac{7}{2}^-$	8.084	0.436

the states decay by single proton emission, and since the higher lying resonances in  $^{15}\text{F}$  can also decay by a two proton emission process, the widths given in Ref. [12] would include effects of that process of decay.

#### IV. $^{14}\text{O}$ SCATTERING FROM HYDROGEN AT $180^\circ$

Using five states in the low excitation spectrum of  $^{14}\text{O}$ , the ground ( $0_1^+$ ), the  $1^-$  (5.17 MeV), the  $0_2^+$  (5.92 MeV), the  $3^-$  (6.27 MeV), and the  $2^+$  (6.59 MeV), MCAS calculations gave the cross sections for  $p$ - $^{14}\text{O}$  scattering at  $180^\circ$  that are compared with data [24] in Fig. 4.

Using semilogarithmic graphing emphasizes small structures in both data and evaluated results. This data clearly indicate three resonances; in [24] they are defined as the  $\frac{1}{2}^+$  ground state of  $^{15}\text{F}$  centered at 1.27 MeV with a width of 0.376 MeV, the  $\frac{5}{2}^+$ , first excited state, with a centroid and width of 2.794 and 0.301 MeV, and a  $\frac{1}{2}^-$  resonance with centroid and width of 4.754 and 0.036 MeV respectively. The calculated results reproduce those three resonances very well. Panel (b) reveals that more structure is predicted for energies in the region above 6 MeV where we anticipate there exist groups of states of both parities. By studying correlations in two proton emission from  $^{16}\text{Ne}$  [13], two resonance aspects of  $^{15}\text{F}$  were defined in that region having centroids at 6.57 and 7.8 MeV excitation. But their spin values and widths are uncertain as yet.

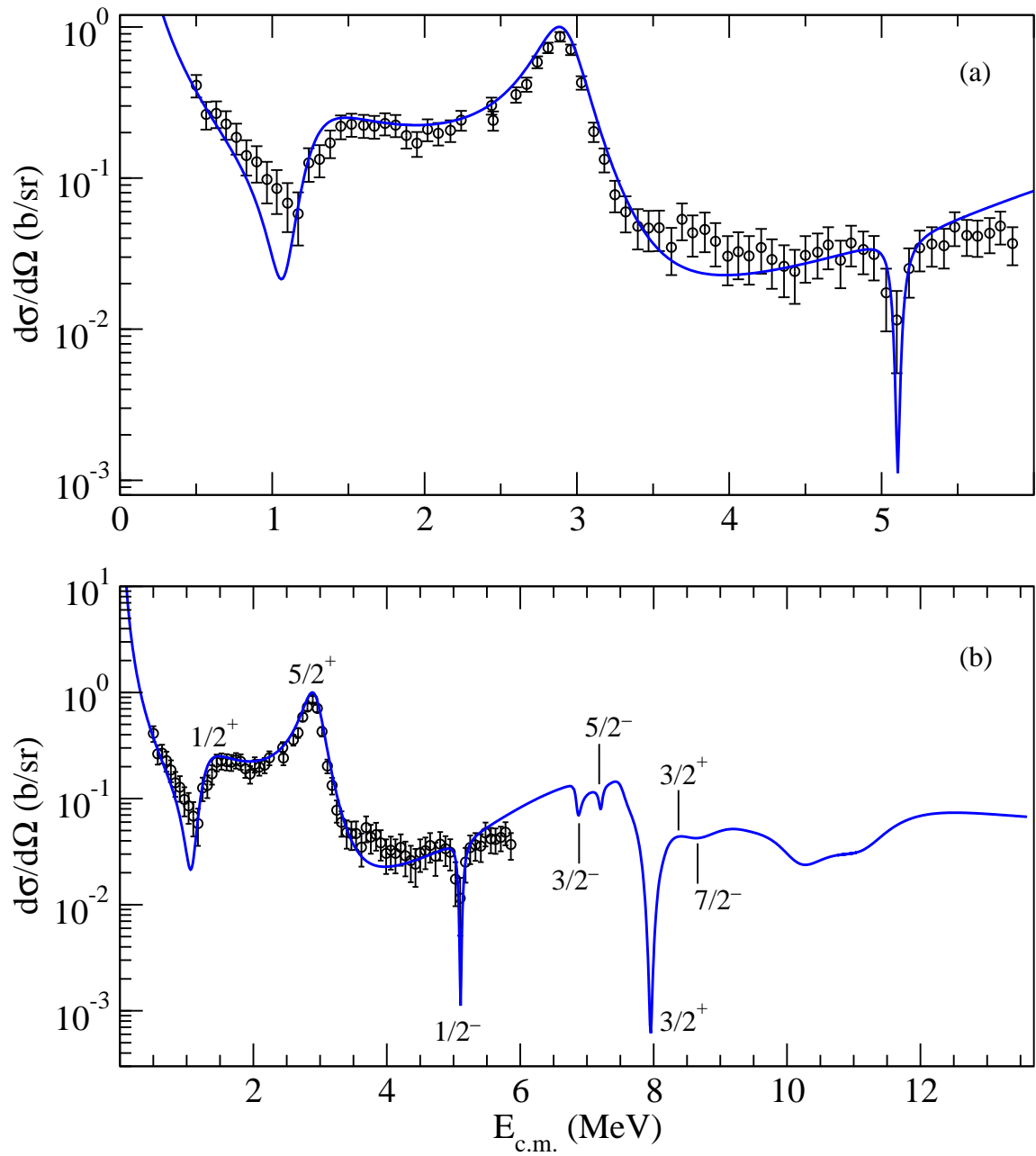


FIG. 4: (a) The  $180^\circ$  cross-section data of [24] compared with MCAS results. The measured data are compared with cross sections evaluated using the vibrational model to specify the matrix of interaction potentials for a proton- $^{14}\text{O}$  cluster. Five states of the core as described in text were used. (b) The same calculation over a larger energy range, predicting resonance features at energies above those measured.

## V. THE MIRROR PAIR $^{15}\text{O}$ ( $n+^{14}\text{O}$ ) AND $^{15}\text{N}$ ( $p+^{14}\text{C}$ )

Being strongly bound, the spectra of the mirror pair,  $^{15}\text{O}$  and  $^{15}\text{N}$ , have been studied for many decades [43]. That of the better known,  $^{15}\text{N}$ , was recently surveyed experimentally over a range of 15 MeV using the  $^{14}\text{N}(d,p)^{15}\text{N}$  reaction [44], and in the same paper the COSMO shell model code [45] was used to successfully calculate these levels, up to 11.5 MeV. That investigation used an unrestricted  $1p-2s1d$  shell valence space. Mirror states in the less-well-known  $^{15}\text{O}$  spectrum were then suggested. Another shell model investigation using a lesser space, the  $2s_{1/2}$  and  $1d_{5/2}$  shells, soon followed [46].

Using MCAS, the nuclear interactions for the  $n+^{14}\text{O}$  and  $p+^{14}\text{C}$  systems are stronger than those required with the  $p+^{14}\text{O}$  and  $n+^{14}\text{C}$  calculations. That is evident from the much larger energies (13.223 and 10.207 MeV) of the relevant nucleon-core nucleus thresholds above the ground states of  $^{15}\text{O}$  and  $^{15}\text{N}$  respectively. That expectation also follows from the numbers of strong attractive (8), versus those of repulsive (6), two-nucleon interactions experienced by the extra-core nucleon in the clusters,  $^{15}\text{N}$  ( $p+^{14}\text{C}$ ) and  $^{15}\text{O}$  ( $n+^{14}\text{O}$ ). In the clusters,  $^{15}\text{C}$  ( $n+^{14}\text{C}$ ) and  $^{15}\text{F}$  ( $p+^{14}\text{O}$ ), in contrast there are 6 strong attractive and 8 repulsive pairings. Additionally the OPP strengths for the  $^{15}\text{N}$  and  $^{15}\text{O}$  cases will differ from those of the  $^{15}\text{C}$  and  $^{15}\text{F}$  clusters since, with 6 rather than 8 extra core-like nucleons, the single-nucleon shell occupancies of those nucleons in the core nuclei are lesser.

We have used the MCAS approach to optimally find the sub-threshold levels in  $^{15}\text{O}$  treated as the  $n+^{14}\text{O}$  cluster and especially to find that the ground state lies 13.22 MeV below the neutron emission threshold. This threshold lies well above those for emission of a proton (7.30 MeV), an  $\alpha$  (10.22 MeV) and a  $^3\text{He}$  (12.08 MeV). Thus, while the MCAS calculations lead to 12 sub-threshold (to neutron emission) levels, only the most bound set of 6 are not resonances for emission of the other nuclear particles. Empirically there are 7 actual sub-threshold bound states in  $^{15}\text{O}$  while there are  $\sim 40$  resonant states above those and below the neutron emission threshold. On the other hand, the proton emission threshold in the mirror system,  $^{15}\text{N}$ , is the first of such and lies 10.207 MeV above the ground. Empirically, there are 17 sub-threshold (bound) states in  $^{15}\text{N}$ .

### A. Specifics of the $^{15}\text{O}$ and $^{15}\text{N}$ evaluations using MCAS

The nuclear interaction and the OPP weights to account for Pauli blocking of single nucleon states was specified by finding as good a spectrum for  $^{15}\text{O}$  ( $n+^{14}\text{O}$ ) as possible. In particular, we sought the ground state of correct spin-parity and energy below the neutron emission threshold and the first two excited states in the correct

order and with good energy values. The coupled-channel Hamiltonian was formed using the five states of the target nucleus  $^{14}\text{O}$  as used before (and of  $^{14}\text{C}$  in the case of  $^{15}\text{N}$ ). The geometry,  $V_{ls}$ , and  $V_{ll}$  values were set at those determined from our MCAS study of the other mass-15 isobars,  $^{15}\text{C}$  and  $^{14}\text{F}$ . However, for the reasons discussed above, the central interaction strength was varied with  $-57.0$  MeV found appropriate. The parameter values of the OPP used for the two systems are listed in Table IV.

TABLE IV: Parameter values defining the  $n+^{14}\text{O}$  and  $p+^{14}\text{C}$  interaction interactions.  $\lambda$  are blocking strengths of occupied single nucleon orbits, in MeV.

		Odd parity	Even parity		
$V_0$ (MeV)		-57.0	-57.0		
$V_{ll}$ (MeV)		0.475	0.475		
$V_{ls}$ (MeV)		7.0	7.0		
$V_{ss}$ (MeV)		0.0	0.0		
		$R_0$ (fm)	$a$ (fm)	$\beta_2$	$\beta_3$
		3.083	0.63	-0.36	-0.48
$J^\pi$	E $^{14}\text{O}$	E $^{14}\text{C}$	$\lambda_{0s_{\frac{1}{2}}}$	$\lambda_{0p_{\frac{3}{2}}}$	$\lambda_{0p_{\frac{1}{2}}}$
$0_1^+$	(0.00)	(0.00)	$10^6$	17.5	2.8
$1_1^-$	(5.17)	(6.09)	$10^6$	17.5	1.25
$0_2^+$	(5.92)	(6.59)	$10^6$	17.5	3.5
$3_1^-$	(6.27)	(6.78)	$10^6$	17.5	1.6
$2_1^+$	(6.59)	(7.01)	$10^6$	17.5	1.7

For the  $^{15}\text{N}$  calculation Coulomb interactions have been added to the nuclear ones and the appropriate set of state energies in  $^{14}\text{C}$  used. In this case, the Coulomb interactions were constrained by using a charge distribution that matches the known root-mean-square (rms) charge radius. For  $^{14}\text{C}$  that value is  $R_{\text{rms}}^{(c)} = 2.56 \pm 0.05$  fm [39], defined using a modified Harmonic Oscillator (MHO) model for the charge distribution of  $^{14}\text{C}$  to analyze electron scattering form factor in the momentum range 1.04 to 2.16  $\text{fm}^{-1}$ .

We have used the three parameter Fermi (3pF) model for the charge distribution. Sets of parameter values ranging between those reported [39] from analyses of electron scattering data from  $^{12}\text{C}$  and from  $^{16}\text{O}$  were determined by the distributions having the charge rms radius of 2.56 fm for  $^{14}\text{C}$ . That set of parameters are listed in Table V. The first three parameter sets, (a), (b), and (c) in Table V are one parameter variations on the 3pF model parameters for the adopted charge distribution in  $^{12}\text{C}$  [39] that give  $R_{\text{rms}}^{(c)} = 2.56$  fm. The set, (d), (e), and (f), kept  $R_c = 2.344$  fm, varied  $a_c$  and adjusted  $w_c$  to find the same  $R_{\text{rms}}^{(c)}$ . The last set in Table V kept  $a_c = 0.5$  fm varied  $R_c$  and adjusted  $w_c$  to have the same result. Thus there are quite diverse sets of parameters for this model giving the known rms charge radius. As shown in Refs. [18, 40], it is the value of  $R_{\text{rms}}^{(c)}$  that affects the



TABLE V: Parameter values for a 3pF model of the charge distribution in  $^{14}\text{C}$  that give  $R_{\text{rms}}^{(c)} = 2.56$  fm and the ground state energies from MCAS calculations of the  $p+^{14}\text{C}$  system.

ID	$R_c$ fm.	$a_c$ fm.	$w_c$	$E_{\text{g.s.}}(^{15}\text{N})$
(a)	2.355	0.5224	-0.08	-10.200
(b)	2.355	0.6	-0.149	-10.209
(c)	2.52	0.5224	-0.149	-10.206
(d)	2.355	0.5	-0.04	-10.199
(e)	2.355	0.54	-0.1	-10.203
(f)	2.355	0.64	-0.15	-10.232
(g)	2.425	0.5	-0.06	-10.208
(h)	2.525	0.5	-0.09	-10.222
(i)	2.536	0.5	-0.1	-10.220

Coulomb potential, with the specific values of  $R_c$ ,  $a_c$ , and  $w_c$  leading to that  $R_{\text{rms}}^{(c)}$  being only of minor impact on results. MCAS evaluations using each of these 3pF sets were made and the spectra found were all very similar. The last column in Table V lists the value of the ground state energies showing a difference of at most 20 keV.

### B. The spectra of $^{15}\text{O}$ and $^{15}\text{N}$

The low-excitation spectra of the mirror pair,  $^{15}\text{O}$  and  $^{15}\text{N}$ , are depicted in Fig. 5. Those for  $^{15}\text{O}$  are shown on the left and those for  $^{15}\text{N}$  on the right. The excitation energies are shown relative to the nucleon separation thresholds (13.223 MeV for  $n+^{14}\text{O}$  and 10.207 MeV for  $p+^{14}\text{C}$ ). The calculated spectrum for  $^{15}\text{N}$  displayed was found using the 3pF model parameter set ‘(h)’ in Table V. The known states are given in the columns labelled ‘exp’ were taken from [32] and the calculated spectra are identified by the label ‘MCAS’.

The results for  $^{15}\text{O}$  closely match most known states to 10 MeV excitation though there are many more levels that lie  $\sim 10$  MeV and greater above the ground. Notably, the ground state is found to within a keV of its known energy below the neutron emission threshold, the doublet of states at  $\sim -8$  MeV binding are found in the correct order, and the next five known states in the spectrum have calculated partners with energies within a few hundred keV of the known values.

With that nuclear interaction, using the appropriate energies of the same five target states (in  $^{14}\text{C}$ ), and the 3pF charge distribution with the parameters of set ‘(h)’ in Table V, the single run of MCAS then lead to the spectrum for  $^{15}\text{N}$  that is compared with the known one in the right side of Fig. 5. The ground state was found to be -10.22 MeV below the neutron emission threshold, in good agreement with the known value, and the low lying spectrum again reasonably matched. The  $\frac{5}{2}^+|_1$  state now is more bound than the  $\frac{1}{2}^+|_1$  one, as is the case in the experimental spectrum, and the splitting of that

doublet is larger than observed. The next two states in the known spectrum of  $^{15}\text{N}$  have matching partners from the calculation, both lying within a few hundred keV of the appropriate energies. Also the known  $\frac{7}{2}^+$  state has a calculated partner in close agreement but the  $\frac{5}{2}^+|_2$  state is calculated to be at  $\sim -0.5$  MeV, not at  $\sim -3$  MeV in the experimental spectrum.

The known spectra of both mass-15 isobars are much richer than those we have evaluated but only for reasonably large excitations reflecting the simplicity of the model chosen to define the coupled-channel Hamiltonian; with the number of core nuclear states used and use of the purest of vibration models for the structure and interactions.

## VI. CONCLUSIONS

Mirror symmetry for nuclear interactions was used to study the spectra of the mass-15 isobars,  $^{15}\text{C}$ ,  $^{15}\text{N}$ ,  $^{15}\text{O}$ , and  $^{15}\text{F}$ . The MCAS method has been used to evaluate their low energy (to  $\sim 10$  MeV) excitation spectra considering each to be a cluster of a nucleon with either of the mirrors,  $^{14}\text{C}$  and  $^{14}\text{O}$ . There are two mirror pairs in these mass-15 isobars,  $^{15}\text{O}$  and  $^{15}\text{N}$ , and  $^{15}\text{C}$  and  $^{15}\text{F}$ , which are distinct in that the former are well bound with many uniquely bound states in their spectra, while of the latter pair  $^{15}\text{C}$  is weakly bound with just two sub-threshold states and its mirror,  $^{15}\text{F}$ , lies beyond the proton drip-line.

In the evaluations, the lowest five states in the core nuclei,  $^{14}\text{C}$  and  $^{14}\text{O}$ , were used to form coupled-channel interactions based upon a collective (vibration) model description of the core nuclei. First we sought the spectra of  $^{15}\text{C}$  (as the  $n+^{14}\text{C}$  cluster). With the set of parameter values for the Hamiltonian that gave a best match to the known spectrum of  $^{15}\text{C}$  (to  $\sim 6.5$  MeV excitation, on addition of Coulomb interaction terms, that Hamiltonian lead to a good match to the known spectrum of  $^{15}\text{F}$ . Coulomb interactions for the  $p+^{14}\text{O}$  system were formed from a three parameter Fermi model for the charge distribution in  $^{14}\text{O}$ . The same basic nuclear potential, modified only in central well depth and with OPP strengths reflecting the changes in like-nucleon shell occupancies in the cores, was used to evaluate the spectra of the other mass-15 isobar pair  $^{15}\text{O}$  and  $^{15}\text{N}$ . With this essentially single potential matrix in the Hamiltonians very good agreement was obtained for the low-energy spectra of  $^{15}\text{O}$  and  $^{15}\text{N}$ .

Finally, as the MCAS procedure produces scattering phase shifts for  $^{14}\text{O}(p,p)^{14}\text{O}$  scattering, and in light of recent data, the elastic scattering cross-section calculation reported in a previous letter [8] has been updated. Very good agreement has been found between all three known resonance features and the non-resonant scattering background. These calculated results suggest that scattering cross sections when measured at higher energies (7-9 MeV for example) should reveal more structure

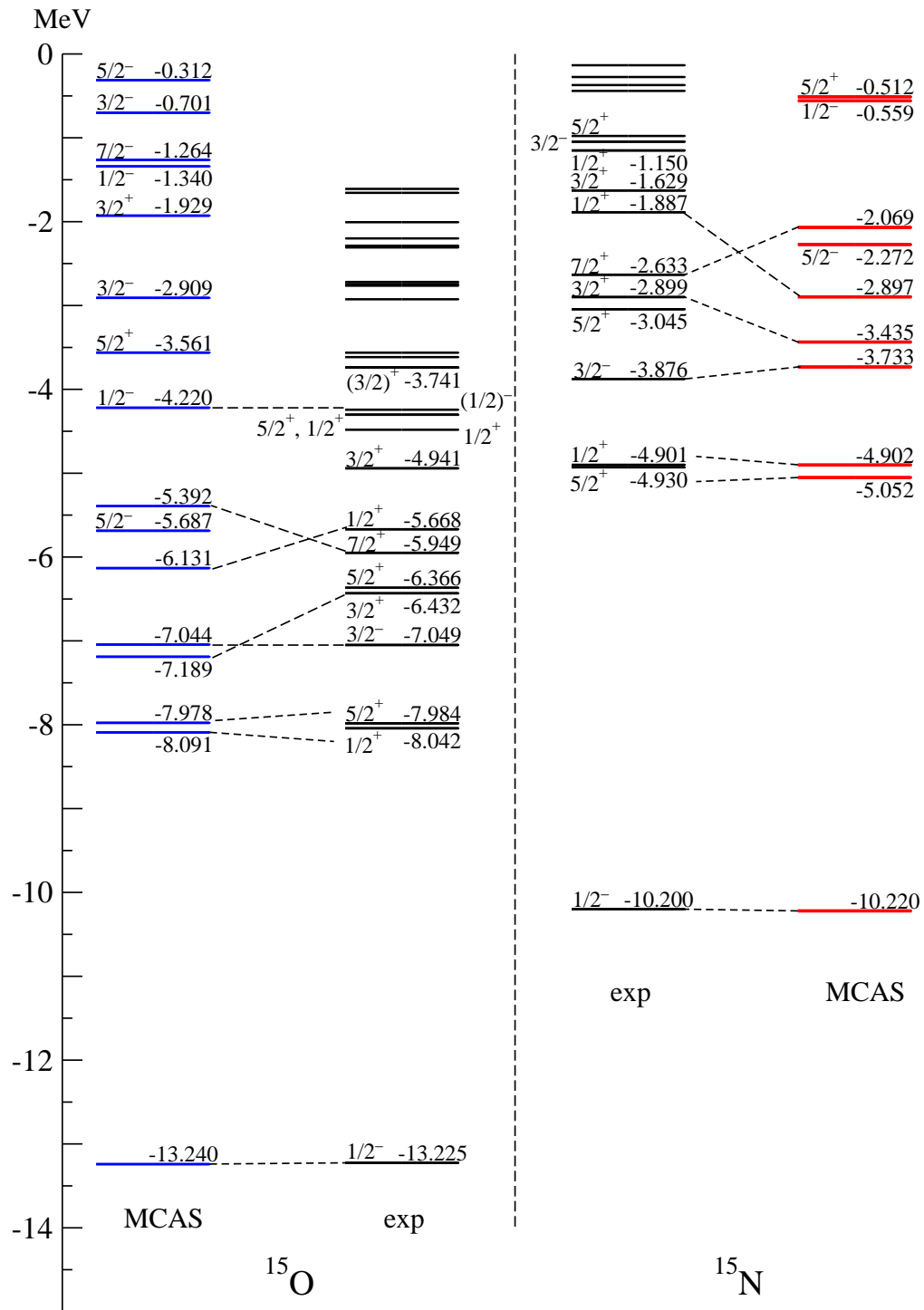


FIG. 5: The sub-threshold spectra of  $^{15}\text{O}$  (left) and of  $^{15}\text{N}$  (right) found using MCAS compared to the experimental values.

(resonance states) in the exotic nucleus,  $^{15}\text{F}$ .

### Acknowledgments

SK acknowledges support from the National Research Foundation of South Africa.

- 
- [1] L. V. Grigorenko, I. G. Mukha, I. J. Thompson, , and M. V. Zhukov, *Phys. Rev. Lett.* **88**, 042502 (2002).
- [2] K. W. Brown et al., *Phys. Rev. Lett.* **113**, 232501 (2014).
- [3] L. V. Grigorenko, T. A. Golubkova, and M. V. Zhukov, *Phys. Rev. C* **91**, 024325 (2015).
- [4] V. Z. Goldberg et al., *Phys. Rev. C* **69**, 031302(R) (2004).
- [5] D. Baye, P. Descouvemont, and F. Leo, *Phys. Rev. C* **72**, 024309 (2005).
- [6] F. Q. Guo et al., *Phys. Rev. C* **72**, 034312 (2005).
- [7] H. T. Fortune and R. Sherr, *Phys. Rev. C* **72**, 024319 (2005).
- [8] L. Canton, G. Pisent, J. P. Svenne, K. Amos, and S. Karataglidis, *Phys. Rev. Lett.* **96**, 072502 (2006).
- [9] H. T. Fortune and R. Sherr, *Phys. Rev. Lett.* **99**, 089201 (2007).
- [10] L. Canton et al., *Phys. Rev. Lett.* **99**, 089202 (2007).
- [11] I. Mukha et al., *Phys. Rev. C* **77**, 061303(R) (2008).
- [12] I. Mukha et al., *Phys. Rev. C* **79**, 061301 (2009).
- [13] I. Mukha et al., *Phys. Rev. C* **82**, 054315 (2010).
- [14] H. T. Fortune, *Phys. Rev. C* **83**, 024311 (2011).
- [15] M. G. Pellegriti et al., *Phys. Lett. B* **659**, 864 (2008).
- [16] F. Wamers et al., *Phys. Rev. Lett.* **112**, 132502 (2014).
- [17] A. Gade et al., *Phys. Lett. B* **666**, 218 (2008).
- [18] P. R. Fraser et al., *J. Phys. G* **43**, 095104 (2016).
- [19] N. K. Timofeyuk et al., *Phys. Rev. C* **86**, 034305 (2012).
- [20] B. Fernández-Domínguez et al., *Phys. Rev. C* **91**, 024307 (2015).
- [21] Y. A. Lashko, G. F. Filippov, and L. Canton, *Ukr. J. Phys.* **60**, 406 (2015).
- [22] F. de Oliveira Santos et al., *AIP Conf. Proc.* **1409**, 134 (2011).
- [23] F. de Oliveira Santos et al., *EPJ Web Conf.* **17**, 06003 (2011).
- [24] F. de Grancey et al., *Phys. Lett.* **B758**, 26 (2016).
- [25] A. Mercenne, Ph.D. thesis, Université de Caen Normandie (2016).
- [26] Y. Jaganathen, N. Michel, and M. Płoszajczak, *Phys. Rev. C* **89**, 034624 (2014).
- [27] L. Canton, G. Pisent, J. P. Svenne, D. van der Knijff, K. Amos, and S. Karataglidis, *Phys. Rev. Lett.* **94**, 122503 (2005).
- [28] K. Amos, L. Canton, P. R. Fraser, S. Karataglidis, J. P. Svenne, and D. van der Knijff, *Nucl. Phys. A* **917**, 7 (2013).
- [29] K. Amos, S. Karataglidis, D. van der Knijff L. Canton, G. Pisent, and J. P. Svenne, *Phys. Rev. C* **72**, 064604 (2013).
- [30] K. Amos, L. Canton, G. Pisent, J. P. Svenne, and D. van der Knijff, *Nucl. Phys. A* **728**, 65 (2003).
- [31] P. Fraser et al., *Phys. Rev. Lett.* **101**, 242501 (2008).
- [32] F. Ajzenberg-Selove, *Nucl. Phys.* **A523**, 1 (1991).
- [33] L. Canton et al., *Phys. Rev. C* **83**, 047603 (2011).
- [34] P. R. Fraser et al., *Phys. Rev. C* **94**, 034603 (2016).
- [35] Y. H. Lam, N. A. Smirnova, and E. Caurier, *Phys. Rev. C* **87**, 054304 (2013), (and references cited therein).
- [36] S. Karataglidis, Ph.D. thesis, The University of Melbourne (1995).
- [37] S. Raman, C. W. Nestor, and P. Tikkanen, *At. Data and Nucl. Data Tables* **78**, 1 (2001).
- [38] R. H. Spear, *At. Data and Nucl. Data Tables* **42**, 55 (1989).
- [39] H. de Vries, C. W. de Jager, and C. de Vries, *At. Data and Nucl. Data Tables* **36**, 495 (1987).
- [40] P. R. Fraser et al., *Eur. Phys. J. A* **51**, 110 (2015).
- [41] J. P. Svenne, L. Canton, K. Amos, P. R. Fraser, S. Karataglidis, G. Pisent, and D. van der Knijff, *Phys. Rev. C* **95**, 034305 (2017).
- [42] J. Kelley, T. Truong, and C. G. Sheu, *ENSDF* (17/07/16).
- [43] L. D. Wyly, *Phys. Rev.* **76**, 316 (1949).
- [44] C. E. Mertin, D. D. Caussyn, A. M. Crisp, et al., *Phys. Rev. C* **91**, 044317 (2015).
- [45] A. Volya, *Phys. Rev. C* **79**, 044308 (2009).
- [46] H. T. Fortune, *Phys. Rev. C* **94**, 024339 (2016).